HHS Public Access

Author manuscript

*Pharm Res*. Author manuscript; available in PMC 2019 January 05.

Published in final edited form as:

*Pharm Res*. ; 35(1): 19. doi:10.1007/s11095-017-2322-0.

# Semi-Mechanistic Population Pharmacokinetic Modeling of L-Histidine Disposition and Brain Uptake in Wildtype and *Pht1* Null Mice

**Xiao-Xing Wang**[1], **Yang-Bing Li**[2], **Meihua R. Feng**[1], and **David E. Smith**[1]

[1]Department of Pharmaceutical Sciences, College of Pharmacy, University of Michigan, 428 Church Street, Ann Arbor, Michigan 48109-1065, USA

[2]Department of Medicinal Chemistry, College of Pharmacy, University of Michigan, Ann Arbor, Michigan 48109, USA

## Abstract

**Purpose—**To develop a semi-mechanistic population pharmacokinetic (PK) model to quantitate the disposition kinetics of L-histidine, a peptide-histidine transporter 1 (PHT1) substrate, in the plasma, cerebrospinal fluid and brain parenchyma of wildtype (WT) and *Pht1* knockout (KO) mice.

**Methods—**L-[$^{14}$C]Hisidine (L-His) was administrated to WT and KO mice via tail vein injection, after which plasma, cerebrospinal fluid (CSF) and brain parenchyma samples were collected. A PK model was developed using non-linear mixed effects modeling (NONMEM). The disposition of L-His between the plasma, brain, and CSF was described by a combination of PHT1-mediated uptake, CSF bulk flow and first-order micro-rate constants.

**Results—**The PK profile of L-His was best described by a four-compartment model. A more rapid uptake of L-His in brain parenchyma was observed in WT mice due to PHT1-mediated uptake, a process characterized by a Michaelis-Menten component ($V_{max}$ = 0.051 nmoL/min and $K_m$ = 34.94 μM).

**Conclusions—**A semi-mechanistic population PK model was successfully developed, for the first time, to quantitatively characterize the disposition kinetics of L-His in brain under *in vivo* conditions. This model may prove a useful tool in predicting the uptake of L-His, and possibly other PHT1 peptide/mimetic substrates, for drug delivery to the brain.

### Keywords

brain parenchyma; L-histidine; mice; PHT1; population pharmacokinetics

✉David E. Smith smithb@med.umich.edu.

Meihua R. Feng and David E. Smith contributed equally to this work.

## INTRODUCTION

Proton-coupled oligopeptide transporters (POTs) are responsible for translocating various di/tripeptides and peptidomimetics across biological membranes (1,2). They have a significant influence on the pharmacokinetics (PK) and pharmacodynamics (PD) of their substrates (3–5). To date, four mammalian members of the POT superfamily have been identified, including peptide transporter 1 (PEPT1) and 2 (PEPT2), and peptide/histidine transporter 1 (PHT1) and 2 (PHT2). Unlike PEPT1 and PEPT2, which have been well studied through experiments and modeling approaches (3–5), there is limited information available for PHT1, especially regarding the impact of PHT1 on the PK of its substrates.

PHT1 was first cloned from rat brain in 1997 (6), where it was highly expressed in hippocampus, cerebellum and pontine nucleus, and showed high affinity to L-histidine (L-His) in *Pht1*-transfected *Xenopus laevis* oocytes (6,7). PHT1 was also expressed in a human blood-brain barrier cell line (8). Our preliminary studies in rat and mice showed that PHT1 had a dominant function in brain uptake of the dipeptide substrate glycylsarcosine (9), as well as in regulating the brain distribution of L-His (10). PHT1 has also been found in human and rat intestinal tissue segments (11,12), however, its relevance in substrate absorption is unclear. Moreover, PHT1 expressed in dendritic cells is intimately involved in immunologic diseases related to TLR9 stimulation such as lupus, colitis and persistent viral infection (13–15). Recent genome-wide association studies on systemic lupus erythematosus identified PHT1 variants as an Asian-specific locus for this disease (16–18).

L-His was chosen as a model PHT1 substrate in this study. It is one of the essential amino acids, which can be degraded to many important metabolic products (19). One of the most important metabolites of L-His in the brain is histamine, a neurotransmitter. It is known that histamine has difficulty passing through the barrier systems of the brain (20,21). The production of histamine in the central nervous system (CNS) is not only dependent upon the activity of histidine decarboxylase (HDC) (20), but also on the availability of its precursor, L-His. Therefore, the entry of L-His in brain is correlated with histamine homeostasis (22,23). Brain histamine is produced in histaminergic neuronal and mast cells. There are several transporters responsible for translocating L-His into the brain cells, including L-amino acid transporters (e.g., SNATs, LATs and CATs) and PHT1 (9,12,24–27). However, it appears that PHT1 accounts for 50%of the uptake of L-His, as determined in mouse brain slices, while L-amino acid transporters account for 30% and other unidentified nonsaturable processes for 20% of the uptake (9,10).

Previous studies suggested that PHT1 plays an important role in histidine/histamine homeostasis in brain, as well as in neuropeptide regulation. Thus, understanding the uptake kinetics of PHT1 substrates could facilitate the development of drug delivery strategies for the treatment of neurological diseases related to brain histamine levels. A semi-mechanistic model could provide a useful tool in predicting the brain entry of PHT1 substrates. In order to construct the model, a nonlinear mixed-effects modeling (NONMEM) approach was performed. NONMEM is widely used in analyzing population PK data by virtue of addressing variability with different sources. In this study, a population PK model of L-His was developed in wildtype and *Pht1*-deficient mice. By analyzing and comparing the data

collected from the two genotypes, we were able to characterize the PK properties and relative significance of PHT1 on the *in vivo* disposition of L-His in brain.

## MATERIALS AND METHODS

### Animals

Gender- and age-matched *Pht1*-competent (wildtype or WT) and *Pht1*-deficient (knockout or KO) mice, 8 to 10 weeks of age, were used in this study. The genotype, gender, age and body weight were recorded before the experiments. *Pht1* KO mice were a generous gift of Dr. Noriko Toyama-Sorimachi (15). All animals were bred on a C57BL/6 background (≥99%). The mice were housed in a temperature-controlled environment with 12 h light and dark cycles, and received a standard diet and water *ad libitum* (Unit of Laboratory Animal Medicine, University of Michigan, Ann Arbor, MI). All animal studies adhered to the "Principles of Laboratory Animal Care" by U.S. National Institutes of Health (NIH publication #85-23, revised in 1985).

### *In Vivo* PK and Tissue Distribution of L-His

The *in vivo* PK and tissue distribution data were generated previously in our laboratory (10). In brief, a 100-μl volume of L-[$^{14}$C]His solution (1 nmol/g, 0.4 μCi/mouse) was administrated to WT and *Pht1* KO mice via tail vein injection as a tracer study in which L-[$^{14}$C]His concentrations in plasma were substantially below endogenous L-His concentrations. Blood samples (15–20 μl) were collected serially, via tail nicks, until mice were euthanized at 0.5, 1, 2, 5, 10, 15, 20 and 30 min after dosing. Heparinized blood samples were centrifuged immediately at 3000 g for 3 min at ambient temperature. Radioactivity of the plasma samples was then measured using a dual-channel liquid scintillation counter. CSF samples (5 μl) were obtained from the cisterna magna of mice along with brain parenchyma at specified times (e.g., 2, 5, 10, 20 or 30 min after dosing). The samples were weighed and dissolved in 330 μl of 1 M hyamine hydroxide and incubated overnight at 37°C. An intravenous bolus injection of [$^{3}$H] dextran-MW 70,000 (0.25 μCi/mouse) was administered just prior to harvesting the tissue samples to correct for vascular space.

### Population PK Modeling of L-His in Plasma, CSF and Brain Parenchyma

The concentration-time profiles of these biological fluids and tissue were analyzed using non-linear mixed effects modeling with NONMEM v7.3 (ICON Development Solutions, MD, USA). A subroutine ADVAN6 TRANS1 and the first-order conditional estimation with interaction were used to build the compartment models throughout the modeling procedure. Model development was guided by the likelihood ratio test using objective function values, graphical goodness-of-fit, and non-parametric bootstrap analysis. A stepwise compartmental model building approach was performed in model development to characterize the disposition kinetics of L-His in the plasma, CSF and brain parenchyma. First, a PK model was developed for the plasma concentration-time data, and one-, two-, and three-compartment models were compared. Once this preliminary model was established, the plasma, CSF and brain concentration-time data were fit simultaneously to the structural

model shown in Fig. 1. This schematic model was adopted and modified based on another model (28).

Mass-balance equations for each compartment were shown by the following equations:

For the central and peripheral compartments

$$\frac{\mathrm{dA}_1}{\mathrm{dt}} = -K_{12}\cdot A_1 + K_{21}\cdot A_2 - K_{13}\cdot A_1 + K_{31}\cdot A_3 - \frac{V_{\mathrm{max,PHT}1}\cdot A_1\cdot \mathrm{Genotype}}{K_{m,\mathrm{PHT}1}\cdot V_1 + A_1} - K_{14}\cdot A_1 + K_{41}\cdot A_4 + K_{\mathrm{bulk}}\cdot A_4 - K_{10}\cdot A_1 \quad (1)$$

$$\frac{\mathrm{dA}_2}{\mathrm{dt}} = K_{12}\cdot A_1 - K_{21}\cdot A_2 \quad (2)$$

For the brain parenchyma

$$\frac{\mathrm{dA}_3}{\mathrm{dt}} = K_{13}\cdot A_1 - K_{31}\cdot A_3 + \frac{V_{\mathrm{max,PHT}1}\cdot A_1\cdot \mathrm{Genotype}}{K_{m,\mathrm{PHT}1}\cdot V_1 + A_1} + K_{43}\cdot A_4 - K_{34}\cdot A_3 \quad (3)$$

For the CSF

$$\frac{\mathrm{dA}_4}{\mathrm{dt}} = K_{14}\cdot A_1 - K_{41}\cdot A_4 - K_{\mathrm{bulk}}\cdot A_4 - K_{43}\cdot A_4 + K_{34}\cdot A_3 \quad (4)$$

where $A_1$, $A_2$, $A_3$ and $A_4$ were the amounts of L-His in the central, peripheral, brain parenchyma and CSF compartments, respectively. $V_1$ was the volume of distribution of the central compartment. $K_{10}$, $K_{12}$, $K_{21}$, $K_{13}$, $K_{31}$, $K_{14}$, $K_{41}$, $K_{bulk}$, $K_{34}$ and $K_{43}$ were the first-order micro-rate constants between the respective compartments. *Genotype* was the indicator for the mouse genotype (*Genotype* = 1 for WT, *Genotype* = 0 for KO). Based on expression studies (6,8), L-His entered the brain parenchyma of WT mice via active transport by PHT1 as described by a Michaelis-Menten term ($V_{max,PHT1}$ and $K_{m,PHT1}$) and by other pathways which were simplified as a first-order process ($K_{13}$). There was no PHT1 function in the KO mice. There was passive diffusion of L-His describing its exchange between the brain parenchyma and CSF compartments. Clearance between the brain and CSF compartments ($Q_2$) was assumed to be inversely proportional to the one-half power of molecular weight (*MW*) and estimated by Eq. 5 (28):

$$Q_2 = \frac{0.379}{\sqrt{\mathrm{MW}}} \quad (5)$$

The distribution of L-His between the central and CSF compartments was also assumed to be a first-order process. In addition, L-His was drained from the CSF to central compartment through bulk flow ($Q_{bulk}$). Values for $Q_{bulk}$ and the volumes of distribution for the brain ($V_3$) and CSF ($V_4$) compartments were obtained from the literature (29). Relationships between the micro-rate constants (e.g., $K_{12}$ and $K_{21}$, $K_{34}$ and $K_{43}$, and $K_{bulk}$) and flows (e.g., $Q_1$, $Q_2$ and $Q_{bulk}$) were shown by the following equations:

$$Q_1 = V_1 \cdot K_{12} = V_2 \cdot K_{21} \quad (6)$$

$$Q_2 = V_3 \cdot K_{34} = V_4 \cdot K_{43} \quad (7)$$

$$Q_{\text{bulk}} = V_4 \cdot K_{\text{bulk}} \quad (8)$$

Inter-animal variability (IIV) of the PK parameters was assumed to follow a log-normal distribution and described by an exponential error model. Additive, proportional and mixed error models were evaluated for the residual unexplained variability. The impact of genotype, gender, age and body weight of animal on PK parameters was evaluated. IIVs and covariates were included in the model only if they were associated with a decrease in OFV by at least 3.84 ($\chi^2$ $p$ value ≤ 0.05).

The final PK model was evaluated by nonparametric bootstrap analyses and visual predictive checks using Perlspeaks-NONMEM (PsN 4.2.0). Two hundred bootstrap samples were generated from the original data set and then fitted to the final population PK model to obtain parameter estimates. The median and 90% bootstrap confidence interval calculated from the successful bootstrap runs were compared with the final model estimates. For visual predictive checks, 1000 hypothetical datasets were simulated using the parameter estimates of the final model. The 90% prediction intervals were calculated and checked by visual inspection to see how the intervals overlapped with the observed data.

### Statistics

Experimental results were reported as mean ± SE. A two-tailed unpaired Student's t-test was used to determine statistical differences between two treatment groups. A $p$ value ≤0.05 was considered significant.

## RESULTS

### Differential Brain Biodistribution of L-His in WT and *Pht1* KO Mice

As shown in Fig. 2, brain L-His concentrations were significantly lower in *Pht1* KO mice compared to WT animals at early time points (before 10 min) but less so at later ones, suggesting a difference on the distribution rate of L-His from the plasma to brain. The plasma and CSF concentration-time profiles of L-His were comparable in the two

genotypes. Based on these findings, genotype differences would be considered a covariate for the uptake rate constant of L-His in brain.

### Population PK Modeling of L-His in Plasma, CSF and Brain Parenchyma

A stepwise compartmental model building approach was performed to characterize the disposition kinetics of L-His in the plasma, CSF and brain parenchyma. The disposition kinetics of L-His in plasma was best described by a two-compartment model. The expanded four-compartment model, including brain parenchyma and CSF, is shown in Fig. 1. The estimated PK parameters and bootstrap results were listed in Table I. Consistent with our previous noncompartmental analysis (10), the plasma PK parameters of L-His were comparable in WT and *Pht1* KO mice. The total plasma clearance (CL) of L-His was 0.30 mL/min, and its volumes of distribution in the central ($V_1$) and peripheral ($V_2$) compartments were 4.52 mL and 5.55 mL, respectively. The distribution kinetics between plasma and CSF compartments were also similar in the two genotypes. A more rapid uptake of L-His occurred in the brain parenchyma of WT mice, as compared to *Pht1* KO mice, due to its active transport by PHT1 ($V_{max,PHT1}$ = 0.051 nmoL/min, $K_{m,PHT1}$ = 34.94 μM), demonstrating that PHT1 plays an important role as an uptake transporter for L-His in brain. In the pilot study, L-His concentrations in brain parenchyma reached a plateau at 20 min post dose, which was consistent with the literature (30). Therefore, we only characterized the first 30 min after dosing, which also minimized the influence of potential metabolites (i.e., nonspecificity of radiolabel) on our results. The first-order rate constant directing L-His from the brain parenchyma to central compartment ($K_{31}$) was fixed as zero in the final model. The impact of mouse genotype, gender, age and body weight on the PK parameters was evaluated. Only genotype was incorporated as a covariate in the final model. An additive error model was used to describe the residual unexplained variability.

### Final Model Validation

Basic goodness-of-fit plots for the final PK model were displayed in Fig. 3. Individual predictions showed a good correlation with observed concentrations in all of the plasma, brain parenchyma and CSF compartments. Conditional weighted residuals randomly distributed along the zero-ordinate line with no obvious deviations. As shown in the visual predicted check plots (Fig. 4), observed concentrations in the plasma and CSF compartments were in good agreement with the prediction intervals of 1000 simulations based on parameter estimates from the final model. However, there was some deviation in the median of predicted values for brain parenchyma in which the observed data were overpredicted at 20min in wildtype mice and underpredicted at 10 and 30 min in *Pht1* null mice. Notwithstanding this finding, nonparametric bootstrap analyses (Table I) showed that all parameter estimates were close to the median and were inside the 90% confidence intervals of the bootstrap estimates.

## DISCUSSION

There is emerging evidence showing that PHT1 plays an important role in the brain as an uptake transporter. In particular, the protein expression of PHT1 in brain increased with age in both mice and rats, with its functional activity dominating the uptake of glycylsarcosine in

adult rodent brain slices (9). Moreover, our previous findings have demonstrated that PHT1 was the major transporter in regulating the *in vitro* distribution of L-His in brain, where it accounted for 50% of the total uptake of L-His in hypothalamus slices. In contrast, the L-amino acid transporters accounted for only 30%of the uptake and other nonsaturable pathways for the remaining 20% (10). The brain distribution of L-His *in vivo* was also significantly reduced in *Pht1*-deficient mice, as compared to wildtype mice.

In the present study, the PK properties of PHT1 *in vivo* were characterized for the first time and several new findings were revealed. Specifically, a four-compartment PK model was successfully developed to define the distribution kinetics of the PHT1 substrate L-His from the central compartment to the brain. By comparing wildtype with *Pht1* KO mice, we could quantify the PHT1-mediated active transport of L-His from the plasma to brain *in vivo* with a singleMichaelis-Menten term ($V_{max,PHT1}$ = 0.051 nmoL/min, $K_{m,PHT1}$ = 34.94 μM). Moreover, the similar disposition kinetics of L-His in plasma and CSF between the two genotypes suggested the absence of PHT1 at the blood-CSF and the brain parenchyma-CSF interfaces.

The estimated $K_{m,PHT1}$ value of L-His (34.94 μM) in mice from the final model was close to that reported previously from an *in vitro* experiment of L-His ($K_m$ = 17 μM) in rat *Pht1*-expressing Xenopus oocytes (6). This finding, and their close homology (97% amino acid identity), further adds to the plausibility of the current model regarding the PHT1-mediated plasma-to-brain uptake of L-His. This result from our study also demonstrated that the PHT1 in mouse is a high affinity transporter similar to that in rat (6). PHT1 is widely distributed throughout rat whole brain (6) and expressed in a human blood-brain barrier cell line (8). Therefore, it is possible that PHT1 may contribute to the translocation of L-His from blood to brain parenchyma, as well as from brain extracellular fluid to brain cells. In order to differentiate these two pathways, further investigation is needed, perhaps, by using a microdialysis study design.

As shown in Eq. 3, the uptake of L-His in brain was described by a combination of PHT1-mediated uptake and nonsaturable processes. These processes may reflect passive uptake and/or L-amino acid transporters at the blood-brain barrier, which have Km values in the mM range for SNATs (31) and CATs (32) and 135 μM in RBE4 cells representative of LATs (33), and are assumed not to be saturable in our model. Under linear-conditions (i.e., plasma concentrations << $K_{m,PHT1}$), the rate constant for PHT1-mediated uptake of L-His could be roughly estimated as $V_{max}/(V_1 * K_m)$ = $3.2 \times 10^{-4}$ 1/min. As reported in Table I, the rate constant representing the uptake mediated by other pathways ($K_{13}$) was equal to $16 \times 10^{-4}$ 1/min. Using these numbers, the total first-order plasma-to-brain uptake of L-His would approximately equal $1.9 \times 10^{-3}$ 1/min in wildtype mice, which was close to the literature values of $0.5 - 13.4 \times 10^{-3}$ 1/min, as reported in rat (22,34). Thus, the contribution of PHT1-mediated uptake of L-His in brain was calculated at about 20% *in vivo*, which was smaller than the 50% value determined previously *in vitro* from mouse brain slices (10). Although speculative, this difference may reflect the fact that *in vitro* brain slice results are obtained from a stagnant system, whereas *in vivo* brain results are dynamic and include the temporal aspects of blood flow, membrane residence times and other physiological factors. It

should also be appreciated that the % RSE for $V_{max}$ was high and, if taken into account, the percent contribution of PHT1 could be as high as 30% for the uptake of L-His in brain.

Expression profiling has also revealed the gene expression of *Slc7* and *Slc38* transporters in mouse choroid plexus (35). However, their protein expression levels and functional significance have not been determined. Notwithstanding this uncertainty, the apical location of System N amino acid transporters (and perhaps others) could account for the much greater efflux of L-His from the CSF to central compartment than the reverse (i.e., $K_{41}{\cdot}V_4 > > K_{14}{\cdot}V_1$).

A semi-mechanistic model would be more valuable if we were able to extrapolate these findings in mice to humans. Thus, it would be important to determine the protein expression levels of PHT1 and related transporters in human so that the brain distribution of L-His or future PHT1-substrate drugs could be simulated. Moreover, considering the number of PHT1 variants and their association with lupus systemic erythematosus (16–18), further investigation of PHT1 localization, structure-function and regulation in the brain is warranted.

In conclusion, a semi-mechanistic population pharmacokinetic model was developed that successfully characterized the disposition of L-His, a model PHT1 substrate, in mouse plasma, CSF and brain parenchyma. By modeling the data collected from *Pht1*-competent and *Pht1*-deficient mice simultaneously, we were able to describe for the first time the quantitative contribution of PHT1 in the plasma-to-brain uptake of L-His under *in vivo* conditions. This model may prove a useful tool in predicting the brain distribution of L-His in humans, and PHT1 as a possible target in brain for the delivery of peptide/mimetic therapeutics.

## Acknowledgments

***Acknowledgements and Disclosures*** This work was supported by the National Institutes of Health National Institute of General Medical Sciences grant R01GM115481 (to D.E.S.). Xiao-Xing Wang was supported, in part, by a Rackham Barbour Scholarship from the University of Michigan.

## ABBREVIATIONS

| | |
|---|---|
| **CI** | Confidence interval |
| **CNS** | Central nervous system |
| **CSF** | Cerebrospinal fluid |
| **CV** | Coefficient of variation |
| **CWRES** | Conditional weighted residuals |
| **HDC** | Histidine decarboxylase |
| **IIV** | Inter-individual variability |
| **KO** | Knockout |

| | |
|---|---|
| **L-His** | L-histidine |
| **NONMEM** | Nonlinear mixed-effects modeling |
| **OFV** | Objective function value |
| **PD** | Pharmacodynamics |
| **PEPT** | Peptide transporter |
| **PHT** | Peptide-histidine transporter |
| **PK** | Pharmacokinetics |
| **POT** | Proton-coupled oligopeptide transporter |
| **RSE** | Relative standard error |
| **WT** | Wildtype |

## References


1. Smith DE, Clemencon B, Hediger MA. Proton-coupled oligopeptide transporter family SLC15: physiological, pharmacological and pathological implications. Mol Asp Med. 2013; 34(2–3):323–36.
2. Daniel H, Kottra G. The proton oligopeptide cotransporter family SLC15 in physiology and pharmacology. Pflugers Arch. 2004; 447(5):610–8. [PubMed: 12905028]
3. Huh Y, Hynes SM, Smith DE, Feng MR. Importance of Peptide transporter 2 on the cerebrospinal fluid efflux kinetics of glycylsarcosine characterized by nonlinear mixed effects modeling. Pharm Res. 2013; 30(5):1423–34. [PubMed: 23371515]
4. Xie Y, Shen H, Hu Y, Feng MR, Smith DE. Population pharmacokinetic modeling of cefadroxil renal transport in wild-type and Pept2 knockout mice. Xenobiotica. 2015; 46(4):342–9. [PubMed: 26372256]
5. Yang B, Hu Y, Smith DE. Impact of peptide transporter 1 on the intestinal absorption and pharmacokinetics of valacyclovir after oral dose escalation in wild-type and PepT1 knockout mice. Drug Metab Dispos. 2013; 41(10):1867–74. [PubMed: 23924683]
6. Yamashita T, Shimada S, Guo W, Sato K, Kohmura E, Hayakawa T, et al. Cloning and functional expression of a brain peptide/histidine transporter. J Biol Chem. 1997; 272(15):10205–11. [PubMed: 9092568]
7. Sakata K, Yamashita T, Maeda M, Moriyama Y, Shimada S, Tohyama M. Cloning of a lymphatic peptide/histidine transporter. Biochem J. 2001; 356(Pt 1):53–60. [PubMed: 11336635]
8. Carl SM, Lindley DJ, Das D, Couraud PO, Weksler BB, Romero I, et al. ABC and SLC transporter expression and proton oligopeptide transporter (POT) mediated permeation across the human blood–brain barrier cell line, hCMEC/D3 [corrected]. Mol Pharm. 2010; 7(4):1057–68. [PubMed: 20524699]
9. Hu Y, Xie Y, Keep RF, Smith DE. Divergent Developmental Expression and Function of the Proton-Coupled Oligopeptide Transporters PepT2 and PhT1 in Regional Brain Slices of Mouse and Rat. J Neurochem. 2014; 129(6):955–65. [PubMed: 24548120]
10. Wang XX, Hu Y, Keep RF, Toyama-Sorimachi N, Smith DE. A novel role for PHT1 in the disposition of l-histidine in brain: *In vitro* slice and *in vivo* pharmacokinetic studies in wildtype and Pht1 null mice. Biochem Pharmacol. 2017; 124:94–102. [PubMed: 27845049]
11. Herrera-Ruiz D, Wang Q, Gudmundsson OS, Cook TJ, Smith RL, Faria TN, et al. Spatial expression patterns of peptide transporters in the human and rat gastrointestinal tracts, Caco-2 *in vitro* cell culture model, and multiple human tissues. AAPS Pharm Sci. 2001; 3(1):E9.

12. Bhardwaj RK, Herrera-Ruiz D, Eltoukhy N, Saad M, Knipp GT. The functional evaluation of human peptide/histidine transporter 1 (hPHT1) in transiently transfected COS-7 cells. Eur J Pharm Sci. 2006; 27(5):533–42. [PubMed: 16289537]
13. Baccala R, Gonzalez-Quintial R, Blasius AL, Rimann I, Ozato K, Kono DH, et al. Essential requirement for IRF8 and SLC15A4 implicates plasmacytoid dendritic cells in the pathogenesis of lupus. Proc Natl Acad Sci U S A. 2013; 110(8):2940–5. [PubMed: 23382217]
14. Dosenovic P, Adori M, Adams WC, Pedersen GK, Soldemo M, Beutler B, et al. Slc15a4 function is required for intact class switch recombination to IgG2c in response to TLR9 stimulation. Immunol Cell Biol. 2015; 93(2):136–46. [PubMed: 25310967]
15. Sasawatari S, Okamura T, Kasumi E, Tanaka-Furuyama K, Yanobu-Takanashi R, Shirasawa S, et al. The solute carrier family 15A4 regulates TLR9 and NOD1 functions in the innate immune system and promotes colitis in mice. Gastroenterology. 2011; 140(5):1513–25. [PubMed: 21277849]
16. Han JW, Zheng HF, Cui Y, Sun LD, Ye DQ, Hu Z, et al. Genome-wide association study in a Chinese Han population identifies nine new susceptibility loci for systemic lupus erythematosus. Nat Genet. 2009; 41(11):1234–7. [PubMed: 19838193]
17. Lee HS, Kim T, Bang SY, Na YJ, Kim I, Kim K, et al. Ethnic specificity of lupus-associated loci identified in a genome-wide association study in Korean women. Ann Rheum Dis. 2014; 73(6): 1240–5. [PubMed: 23740238]
18. Wang C, Ahlford A, Jarvinen TM, Nordmark G, Eloranta ML, Gunnarsson I, et al. Genes identified in Asian SLE GWASs are also associated with SLE in Caucasian populations. Eur J Hum Genet. 2013; 21(9):994–9. [PubMed: 23249952]
19. Stifel FB, Herman RH. Histidine metabolism. Am J Clin Nutr. 1971; 24(2):207–17. [PubMed: 4925814]
20. Sakurai E, Sakurai E, Watanabe T, Yanai K. Uptake of L-histidine and histamine biosynthesis at the blood-brain barrier. Inflamm Res. 2009; 58(Suppl 1):34–5. [PubMed: 19271124]
21. Schwartz JC, Arrang JM, Garbarg M, Pollard H, Ruat M. Histaminergic transmission in the mammalian brain. Physiol Rev. 1991; 71(1):1–51. [PubMed: 1846044]
22. Hegstrand LR, Simon JR. Histidine transport into rat brain synaptosomes. J Neurochem. 1985; 45(2):407–14. [PubMed: 3874263]
23. Neame KD. Effect ofAmino Acids on Uptake of L-Histidine byRat Brain Slices. J Neurochem. 1964; 11:67–76. [PubMed: 14125146]
24. Schioth HB, Roshanbin S, Hagglund MG, Fredriksson R. Evolutionary origin of amino acid transporter families SLC32, SLC36 and SLC38 and physiological, pathological and therapeutic aspects. Mol Asp Med. 2013; 34(2–3):571–85.
25. Hagglund MG, Sreedharan S, Nilsson VC, Shaik JH, Almkvist IM, Backlin S, et al. Identification of SLC38A7 (SNAT7) protein as a glutamine transporter expressed in neurons. J Biol Chem. 2011; 286(23):20500–11. [PubMed: 21511949]
26. Usui T, Kubo Y, Akanuma S, Hosoya K. Beta-alanine and l-histidine transport across the inner blood-retinal barrier: potential involvement in L-carnosine supply. Exp Eye Res. 2013; 113:135–42. [PubMed: 23773890]
27. Broer A, Wagner CA, Lang F, Broer S. The heterodimeric amino acid transporter 4F2hc/y+LAT2 mediates arginine efflux in exchange with glutamine. Biochem J. 2000; 349(Pt 3):787–95. [PubMed: 10903140]
28. Kodaira H, Kusuhara H, Fuse E, Ushiki J, Sugiyama Y. Quantitative investigation of the brain-to-cerebrospinal fluid unbound drug concentration ratio under steady-state conditions in rats using a pharmacokinetic model and scaling factors for active efflux transporters. Drug Metab Dispos. 2014; 42(6):983–9. [PubMed: 24644297]
29. Badhan RK, Chenel M, Penny JI. Development of a physiologically-based pharmacokinetic model of the rat central nervous system. Pharmaceutics. 2014; 6(1):97–136. [PubMed: 24647103]
30. Battistin L, Varotto M, Lorenzi AD. Amino acid uptake *in vivo* by the mouse brain and by various regions of the rabbit brain after drug-induced convulsions. Brain Res. 1975; 89(2):215–24. [PubMed: 1148848]

31. Mackenzie B, Erickson JD. Sodium-coupled neutral amino acid (System N/A) transporters of the SLC38 gene family. Eur J Phys. 2004; 447:784–95.

32. Fotiadis D, Kanai Y, Palacín M. The SLC3 and SLC7 families of amino acid transporters. Mol Asp Med. 2013; 34:139–58.

33. Reichel A, Begley DJ, Abbott NJ. Carrier-mediated delivery of metabotropic glutamate receptor ligands to the central nervous system: structural tolerance and potential of the L-system amino acid transporter at the blood-brain barrier. J Cereb Blood Flow Metab. 2000; 20:168–74. [PubMed: 10616805]

34. Vahvelainen ML, Oja SS. Kinetics of influx of phenylalanine, tyrosine, tryptophan, histidine and leucine into slices of brain cortex from adult and 7-day-old rats. Brain Res. 1972; 40(2):477–88. [PubMed: 5027172]

35. Ho HTB, Dahlin A, Wang J. Expression profiling of solute carrier gene families at the blood-CSF barrier. Front Pharmacol. 2012; 3:154. https://doi.org/10.3389/fphar.2012.00154. [PubMed: 22936914]

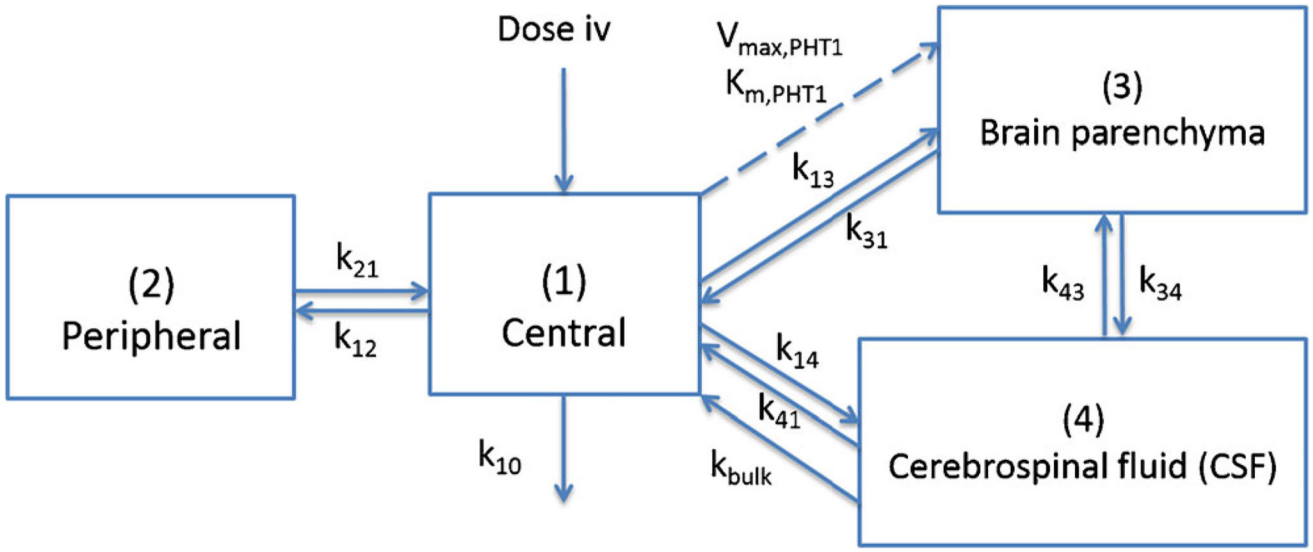


**Fig. 1.**

Schematic structural model of L-histidine disposition in mice after an intravenous (iv) bolus dose. $V_{max,PHT1}$ and $K_{m,PHT1}$, the maximum rate and Michaelis constant of PHT1-mediated active transport of L-histidine from plasma to brain; $k_{10}$, $k_{12}$, $k_{21}$, $k_{13}$, $k_{31}$, $k_{14}$, $k_{41}$, $k_{34}$ and $k_{43}$, the first-order micro-rate constants between the respective compartments; $k_{bulk}$, the first-order micro-rate constant of CSF bulk flow. The dashed line indicates a process existing only in wildtype mice.

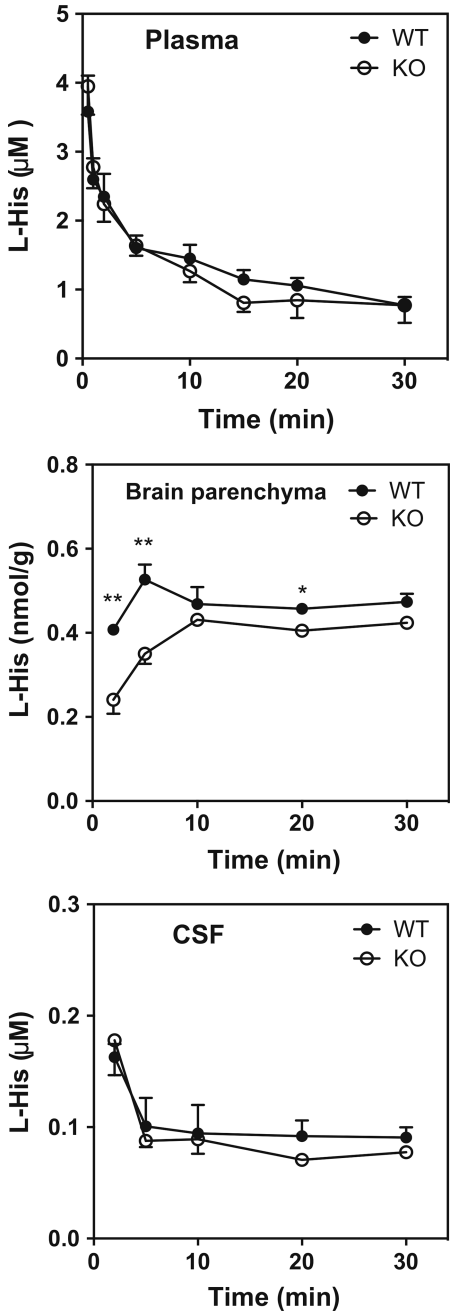


**Fig. 2.**

L-Histidine (L-His) concentration *versus* time plots in plasma, brain parenchyma and CSF compartments of wildtype (WT) and *Pht1* knockout (KO) mice. Data are expressed as mean ± SE ($n$ = 3–6 per time point). *$p \leq 0.05$ and **$p \leq 0.01$. Adapted from a previous paper on L-His disposition in these two genotypes (10).

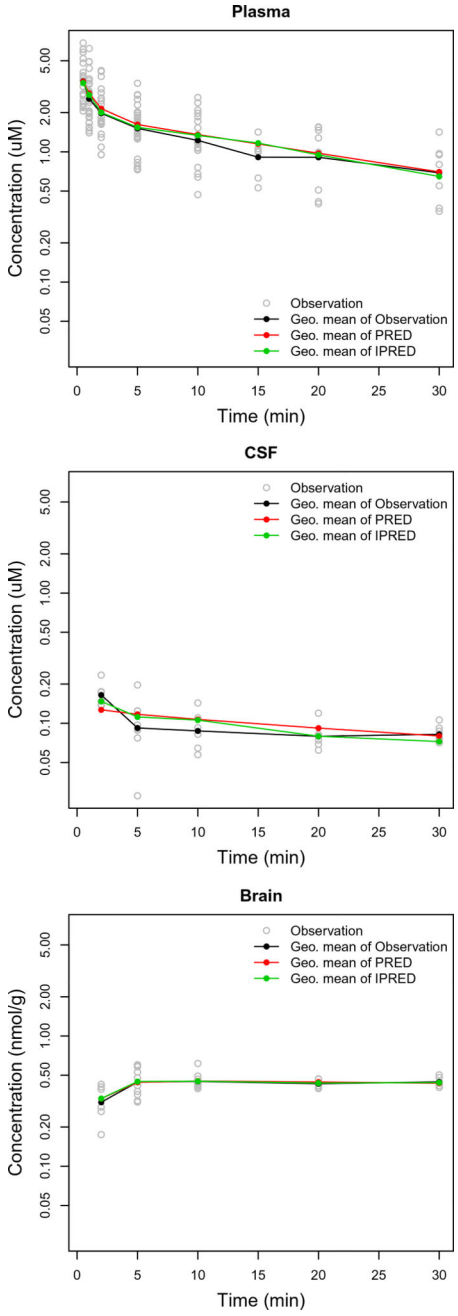

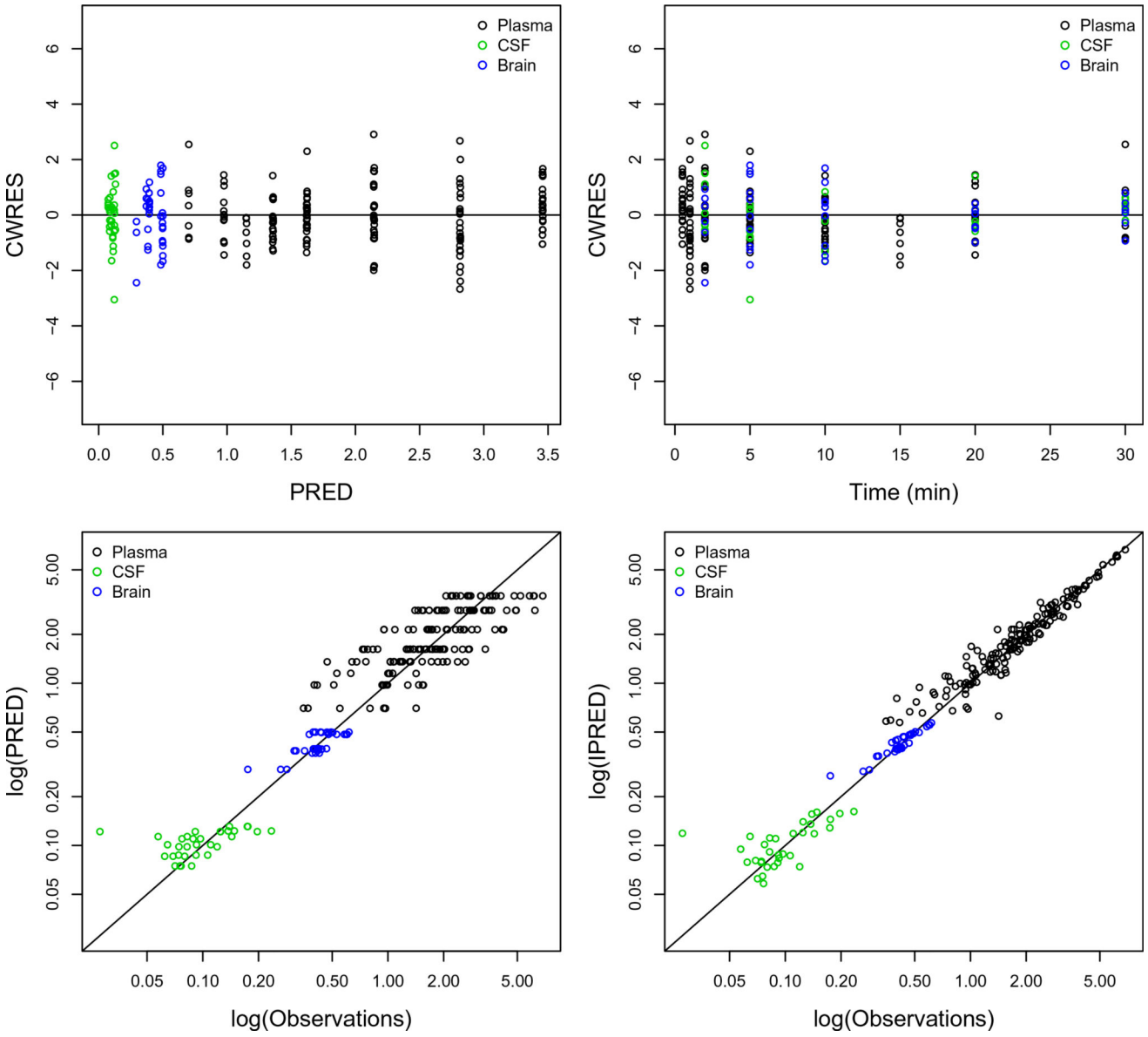


**Fig. 3.**

Basic goodness-of-fit plots for the population pharmacokinetic parameters of L-histidine in plasma, CSF and brain. Geo. mean is the geometric mean, PRED is the population prediction, IPRED is the individual prediction, and CWRES is the conditional weighted residual.

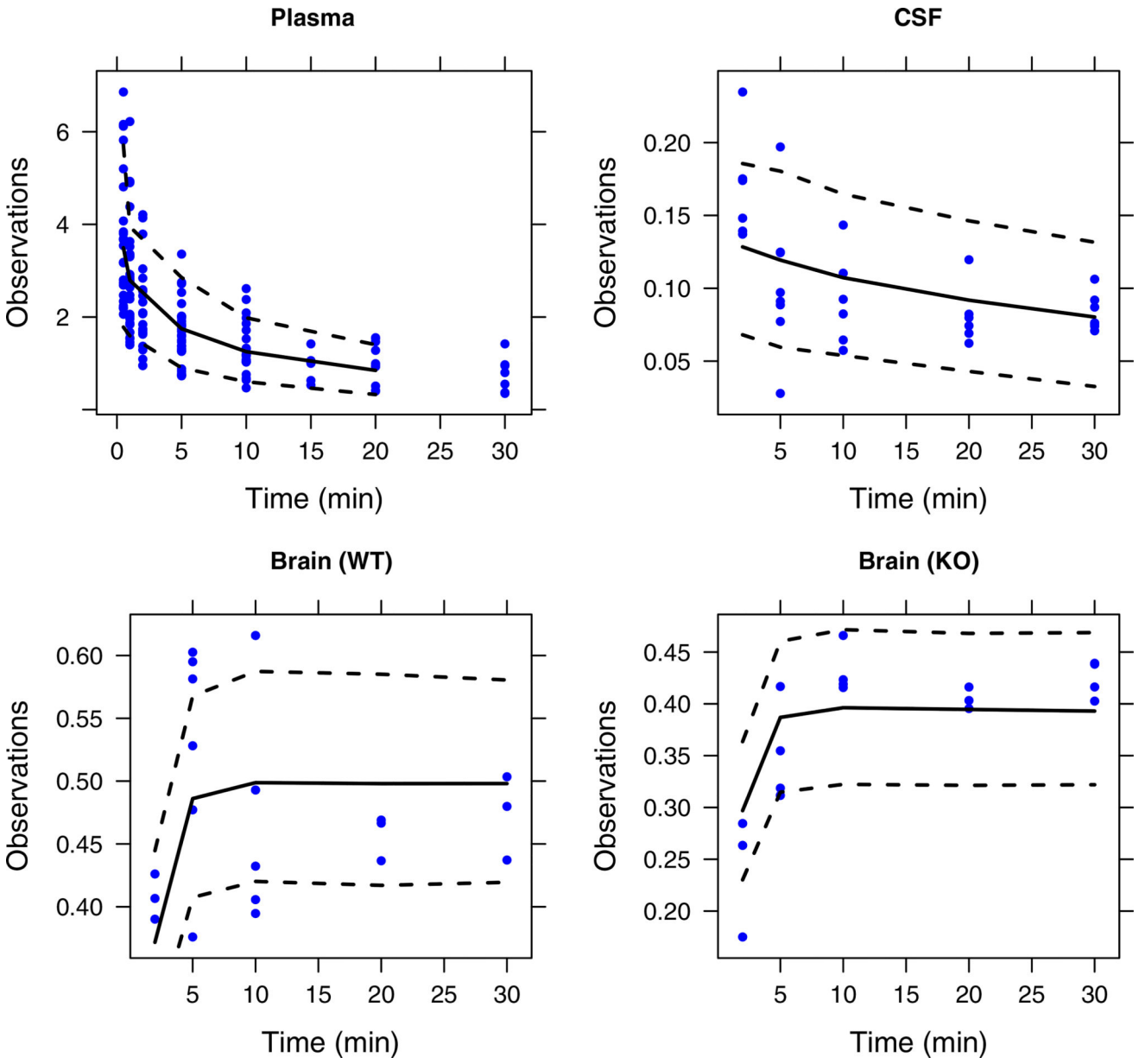


**Fig. 4.**

Visual predictive check for the final pharmacokinetic model of L-histidine in the plasma, CSF and brain of wildtype (WT) and *Pht1* knockout (KO) mice, based on 1000 simulations. Observed data are shown as circles. Solid and dashed lines represent the simulated median, and 10th and 90th percentiles of the simulated data.

## Table I

Population Pharmacokinetics and Bootstrap Results of L-Histidine in Wildtype and *Pht1* Knockout Mice

| Parameters[a] | Estimates (% RSE) | Bootstrap estimates | |
|---|---|---|---|
| | | Median | 90% CI |
| CL (mL/min) | 0.30 (7) | 0.29 | 0.26, 0.33 |
| $V_1$ (mL) | 4.52 (10) | 4.51 | 3.71, 5.30 |
| $V_2$ (mL) | 5.55 (16) | 5.60 | 4.09,6.98 |
| $Q_1$ (mL/min) | 2.12 (8) | 2.13 | 1.87,2.40 |
| $K_{13}$ (1/min) | 0.0016 (13) | 0.0016 | 0.0013,0.0019 |
| $K_{14}$ (1/min) | 0.0013 (26) | 0.0013 | 0.0007,0.0018 |
| $K_{41}$ (1/min) | 1.12 (24) | 1.12 | 0.65,1.56 |
| $K_{m,PHT1}$ (μM) | 34.94 (32) | 34.95 | 17.76, 52.98 |
| $V_{max,PHT1}$ (nmoL/min) | 0.051 (76) | 0.05 | 0.01, 0.11 |
| $V_3$ (mL) | 0.36[b] | | |
| $V_4$ (mL) | 0.09[b] | | |
| $Q_{bulk}$ (mL/min) | 0.000027[b] | | |
| $Q_2$ (mL/min) | 0.00076[c] | | |
| $K_{bulk}$ (1/min) | 0.00030[d] | | |
| $K_{34}$ (1/min) | 0.0021[d] | | |
| $K_{43}$ (1/min) | 0.0084[d] | | |
| IIV[e] % CV (% RSE) | | | |
| ω ($V_1$) | 56 (28) | 56 | 42, 68 |
| ω ($V_2$) | 72 (34) | 71 | 48, 89 |
| RE | | | |
| $\sigma_{plasma}$ (μM) | 0.11 (6) | 0.11 | 0.08,0.14 |
| $\sigma_{brain}$ (μM) | 0.0011 (33) | 0.001 | 0.0005, 0.0017 |
| $\sigma_{CSF}$ (μM) | 0.014 (33) | 0.030 | 0.017, 0.043 |

[a] CL is the total plasma clearance where $CL = V_1 \cdot K_{10}$; $V_1$, $V_2$, $V_3$ and $V_4$ are the respective volumes of distribution in the central, peripheral, brain parenchyma and CSF compartments; $Q_1$, $Q_2$ and $Q_{bulk}$ are the respective clearances between the central and peripheral compartments, brain parenchyma and CSF compartments, and bulk flow from the CSF to central compartment; $K_{13}$, $K_{14}$ and $K_{41}$, and $K_{34}$ and $K_{43}$ are the first-order micro-rate constants between the respective compartments; $K_{bulk}$ is the first-order micro-rate constant from the CSF to central compartment; $K_{m,PHT1}$ is the Michaelis constant for the PHT1-mediated active transport of L-histidine from plasma to brain; Vmax,PHT1 is the maximum rate for the PHT1-mediated active transport of L-histidine from plasma to brain; IIV is the inter-individual variability; RE is the residual error; CV is the coefficient of variation; RSE is the relative standard error; and CI is the confidence interval

[b] Obtained from reference 29

[c] Obtained from Eq. 5 and reference 28

[d] Obtained from $Q_{bulk} = V_4 \cdot K_{bulk}$ and $Q_2 = V_3 \cdot K_{34} = V_4 \cdot K_{43}$

[e] Inter-individual variability was not estimated for $Q_{bulk}$, $Q_2$, $V_3$ and $V_4$